Array-measurements at the broadband-site “SULZ”

G. Stamm, J. Burjanek, D. Fäh
Schweizerischer Erdbebendienst ETH Zürich

Location	Sulz (AG)
Seismic Station	SULZ
Method(s)	H/V-measurements Array-measurements
Date	27/08/2008
Measurements done by	Gabriela Stamm
Processing done by	Gabriela Stamm, Jan Burjanek

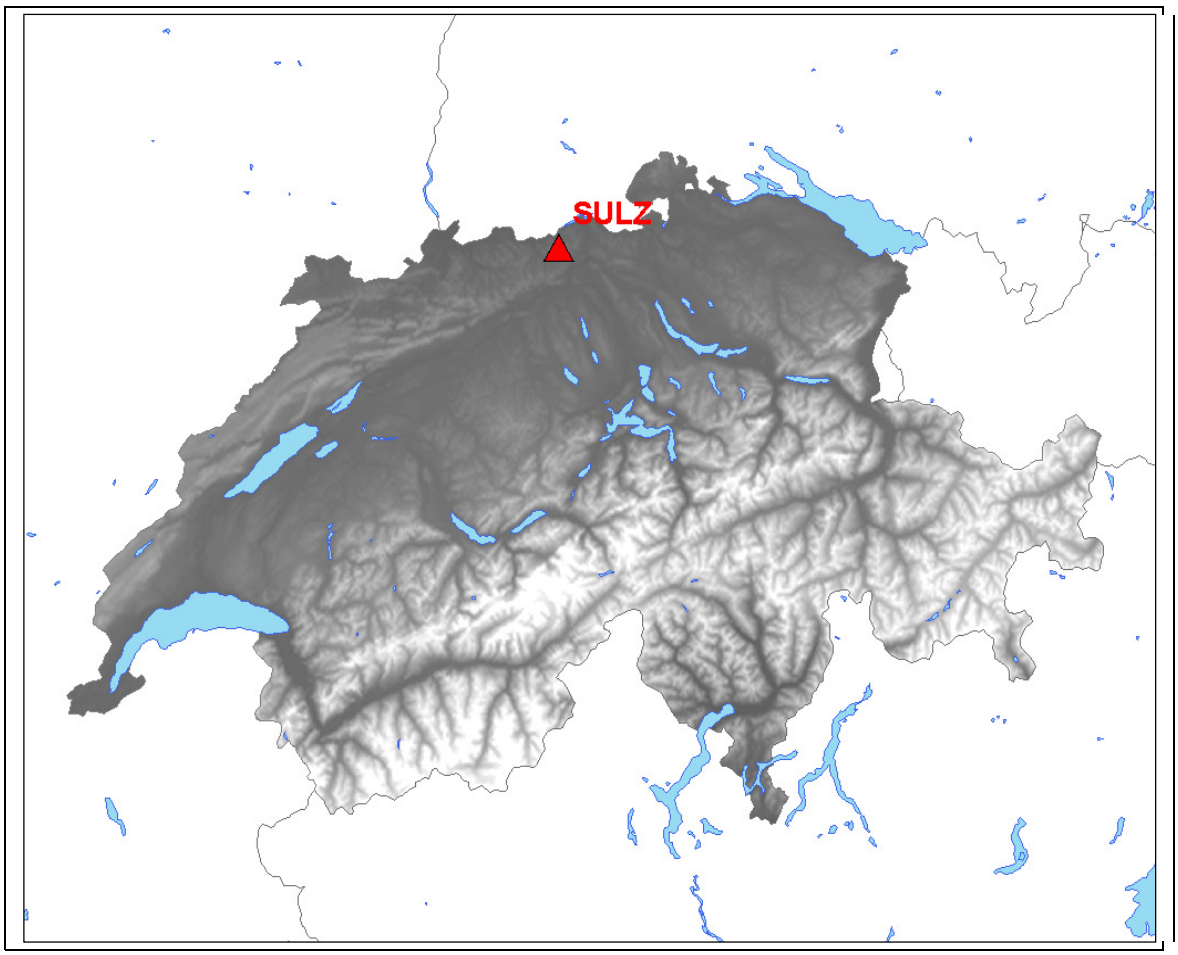

Figure1: *Location of the broadband-site SULZ in Sulz (AG).*

1. Method

H/V

To compute the H/V-ratios, two different methods were applied. The first one is the classical polarisation analysis in the frequency domain, where the polarisation is defined as the ratio between the quadratic mean of the Fourier spectra of the horizontal components and the spectrum of the vertical component. The second method tries to reduce the SH-wave influence by identifying P-SV-wavelets from the signal and taking the spectral ratio only from these wavelets. This is done by means of a frequency-time analysis of each of the three components of the ambient vibrations. Both methods are described in more detail in Fäh et al., 2001. To ensure that the measuring site can be handled as a "1D-case", the H/V-ratios of all array-points were compared together. All points showing differing curves were then excluded of the array-processing.

Array-processing

The first array method we use is based on the high-resolution beam-forming (HRBF) method. It was originally proposed by Capon (1969) but developed and applied to vertical recordings of ambient vibrations by Kind et al. (2005). We have extended this method to also analyse the horizontal components (Fäh et al., 2008). In general, sub-arrays with different apertures are set up for the measurement to optimise the capabilities in a certain frequency band. Small apertures are used to resolve the shallow part of a structure, and by increasing the aperture, deeper and deeper structures can be investigated. The finale dispersion curve over a wide frequency-range is then composed of the parts obtained by the different sub-arrays. The limits of each sub-array are given by the aliasing at high frequencies and the loss of resolution at low frequencies.

In a second step the SPAC method was applied. The Spatial Autocorrelation method is another class of array processing techniques of ambient noise vibrations introduced by Aki (1957). Where both HRBF and SPAC methods have been applied to the same data, SPAC methods have been found to yield higher resolution at low frequencies (Asten, 2006, and references therein). Thus it gives a possibility to increase a bandwidth of the dispersion curves. We use a modified SPAC method for non-circular arrays (Bettig et al., 2001) implemented within GEOPSY software package by Wathelet et al. (2005). Pairs of stations in the array are grouped along rings of certain diameters (the choice of the rings is upon the user). The spatial autocorrelation function is then evaluated for each ring and transformed to the frequency-velocity domain. The so called dispersion density is then generated by stacking SPAC functions in frequency-velocity domain. High density regions should then correspond to dispersion curves.

Inversion

Our inversion scheme is based on a genetic algorithm that was developed by D. Carroll and is described in Fäh et al. (2001, 2003). It does not require explicit starting models but only the definition of parameter limits. To estimate the average S-wave velocity structure below our array, we use the combined H/V spectral ratios and phase velocity curves for Rayleigh- and Love-waves as input.

2. Array-Configuration

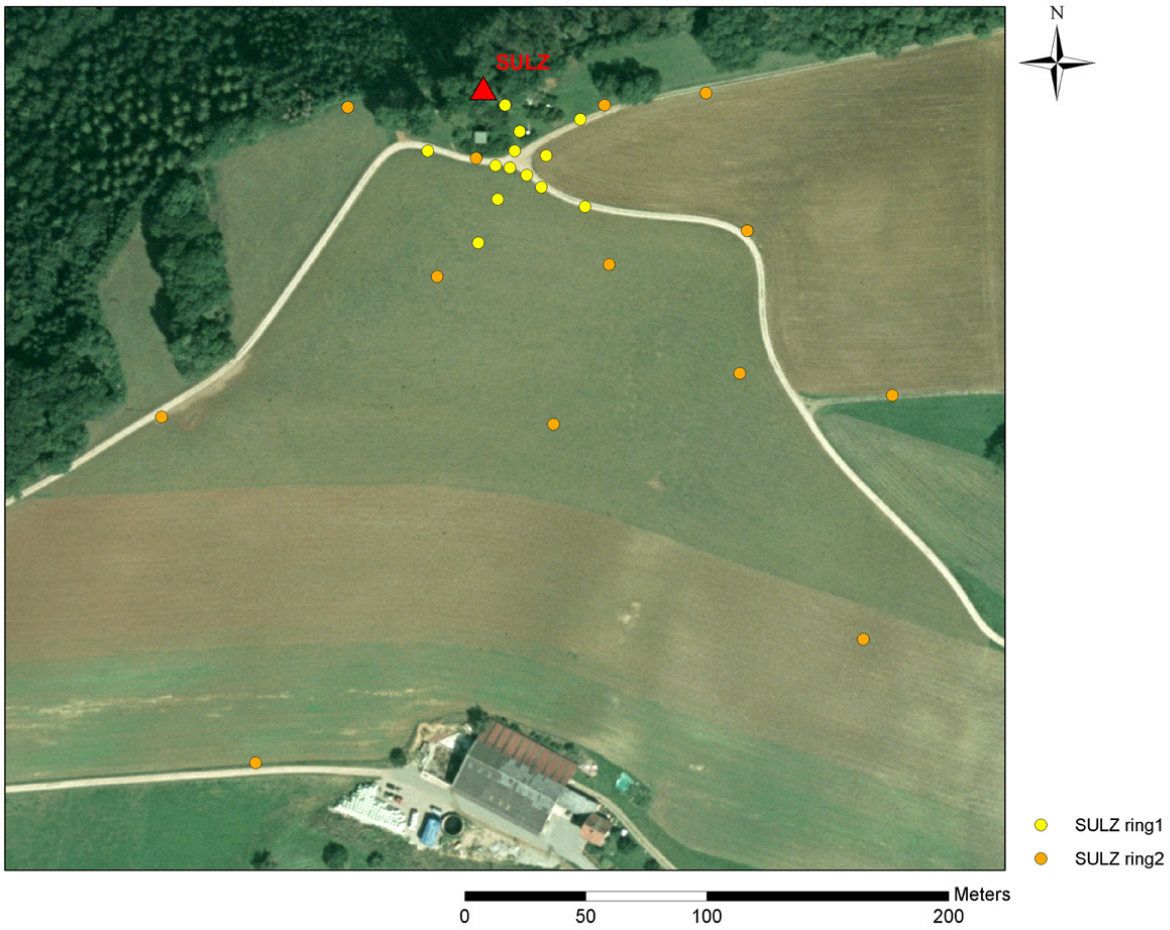

Figure 2: *Array-configuration for SULZ ring1 and ring2.*

Table 1: *Important parameters of the array set ups.*

	SULZ ring1	SULZ ring2
No. Sensors	14	13
max. Radius [m]	35	150
min. distance between two sensors [m]	~7	~70
max. distance between to sensors [m]	~70	~300

The broadband-station SULZ is situated on top of a hill, hence the array was set up on a gentle slope.

3. H/V

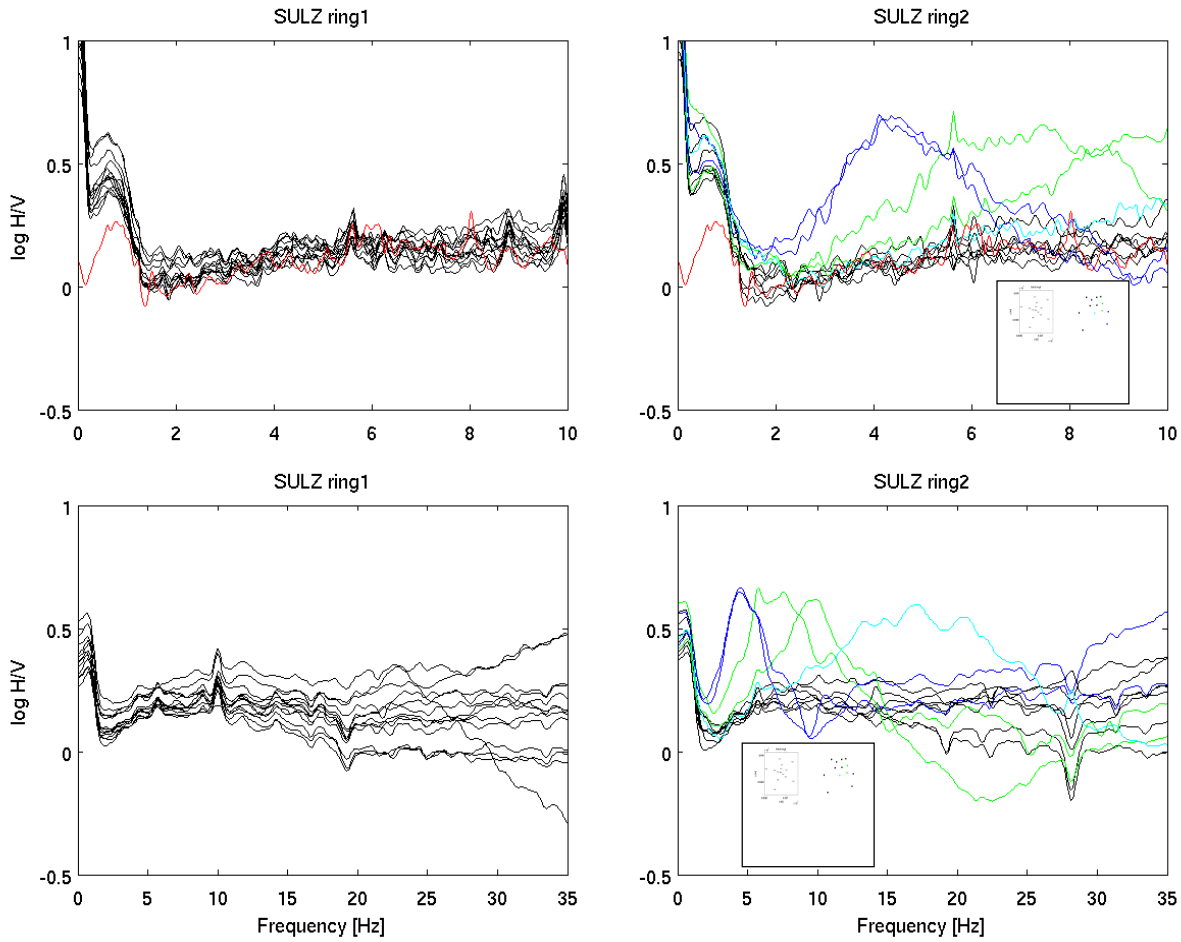

Figure 3: *Comparison of the H/V-ratios of all points measured in SULZ ring1 and ring2 with that from the broadband-station SULZ (red).*

All H/V-ratios of the stations from ring1 are similar, so none of them had to be excluded from the array-processing. By looking at the H/V-ratios of ring2, a change in geology becomes visible. The five stations that are at the south-east of ring2 (see small plots of the array-configuration inside figure 3) show peaks at different frequencies. The further to the east that the stations were situated, the lower the frequency of the peak is. This indicated, that a layer of soft sediments is located to the east with increasing thickness of sediments.

4. Dispersion Curves

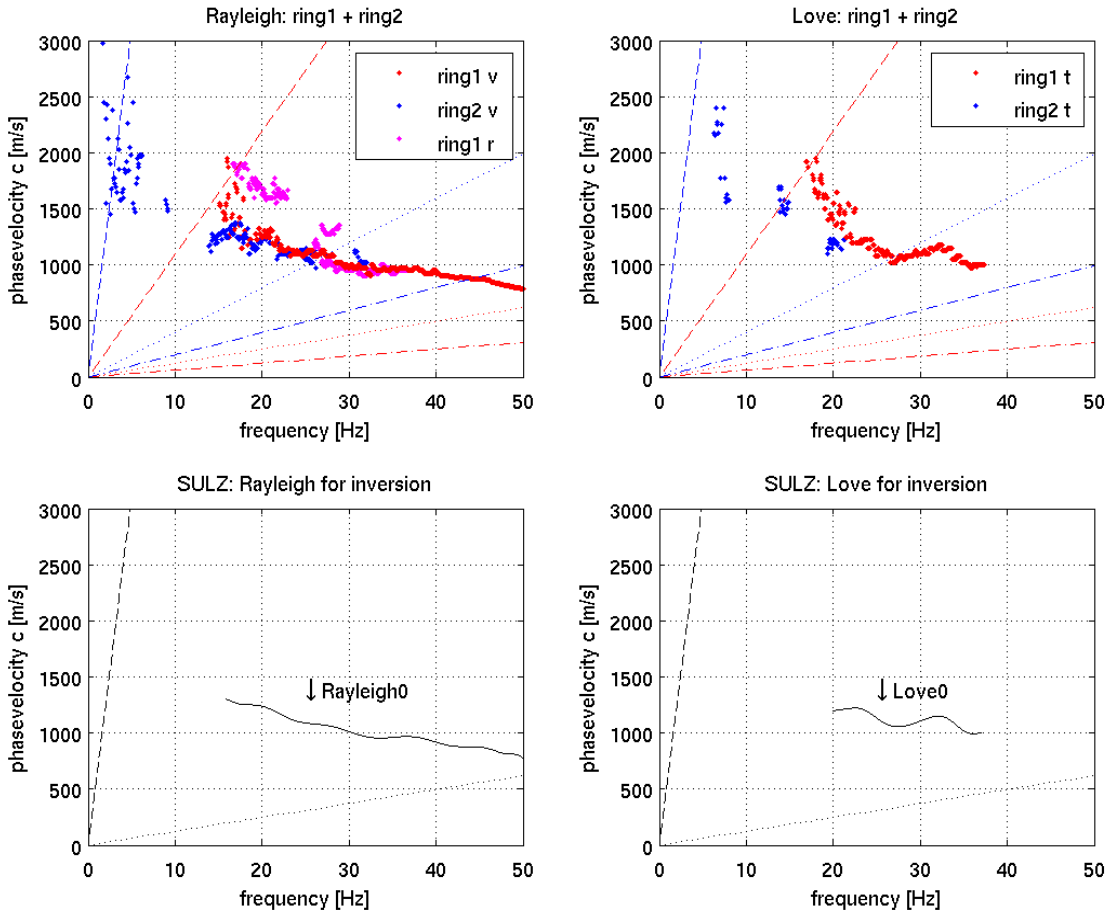

Figure 4: *Rayleigh- and Love-wave dispersion curves for SULZ ring1 and ring2. (v: vertical components, r: radial components, t: transverse components.)*

Dispersion curves were only clearly visible at frequencies higher then 15Hz. On the vertical components of ring1 and ring2 the fundamental mode of Rayleigh-waves is probably visible between 16 and 50Hz. On the radial components of ring1 parts of a higher mode can also be detected. The transverse components of ring1 and ring2 probably show a part of the fundamental mode of Love-waves.

5. Inverted Profiles

Table 1 gives a description of the type of models that were run for the site SULZ. The H/V-ratio was fitted between 0.9-1.3 Hz, the Rayleigh fundamental mode between 16-30 Hz and the Love fundamental mode between 20-30 Hz. Figure 5 shows the obtained S-waves profiles. Figures 6 and 7 show the fit of the theoretical dispersion curves of the inverted models to the observed dispersion curves. The fit is generally good.

Table 1:

	H/V	Rayleigh fund. mode	Love fund. mode
type 1	0.9-1.3Hz	16-30Hz	20-30Hz

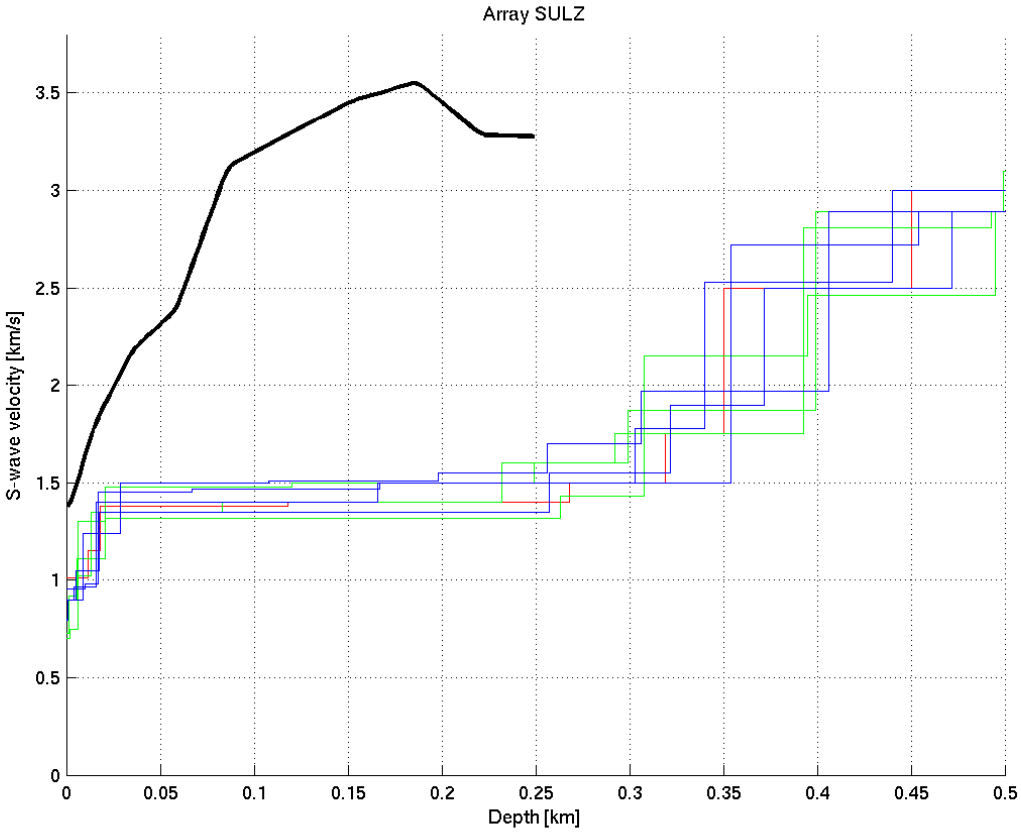

Figure 5: *Inverted S-wave profiles for the site SULZ (coloured curves). The black curve corresponds to the model obtained from seismic measurements by GGA.*

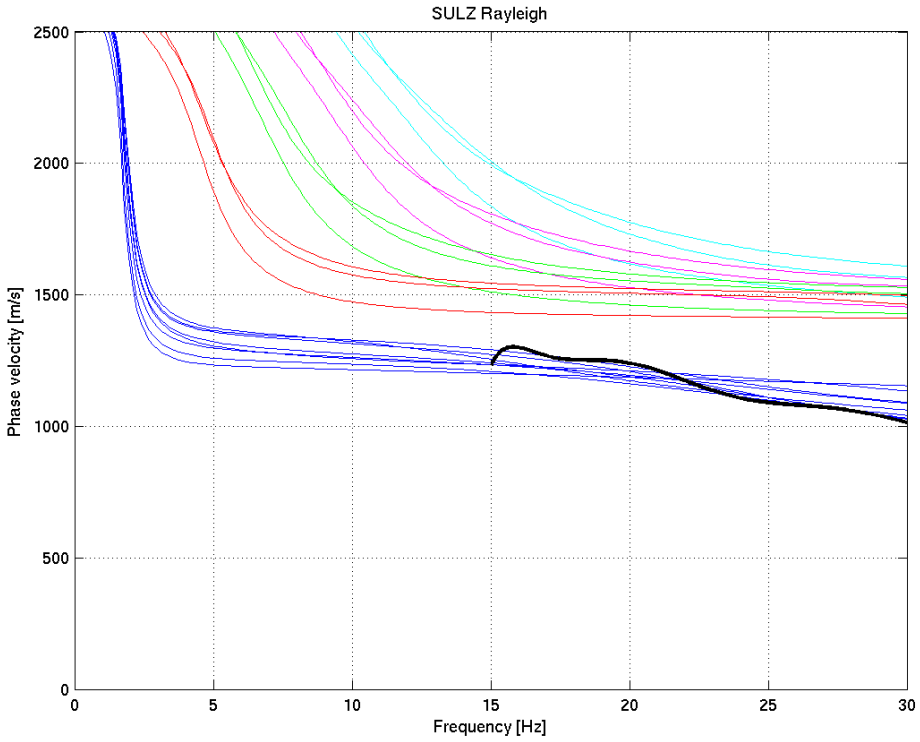

Figure 6: *Comparison between dispersion curves of the inverted structural models and measured curves for Rayleigh waves (colour). Different modes have different colours. The higher modes are not shown for all models.*

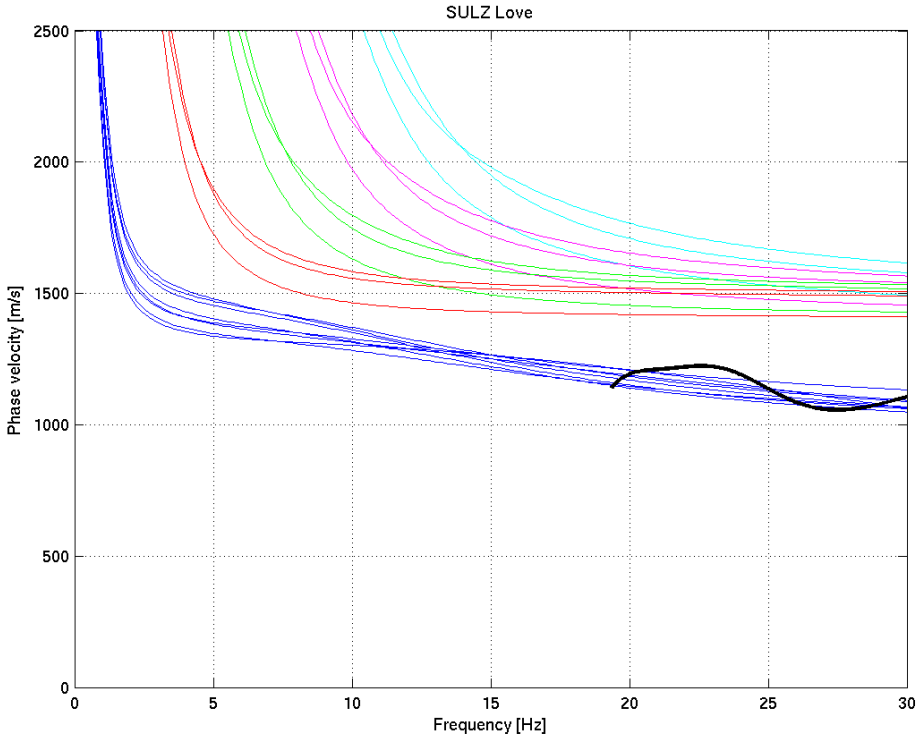

Figure 7: *Comparison between dispersion curves of the inverted structural models and measured curves for Love waves. Different modes have different colours. The higher modes are not shown for all models.*

At the same site S-wave reflection seismic measurements were performed in 2003 by the Institut für Geowissenschaftliche Gemeinschaftsaufgaben (GGA, Germany, unpublished data). The measured mean velocity profile is also shown in Figure 5. Figure 8 shows the measured S-wave velocity profile. The velocities obtained with seismic measurements are much higher than the one's from the ambient vibration array analysis. Such high velocities cannot explain the dispersion curves measured with ambient vibration array measurements.

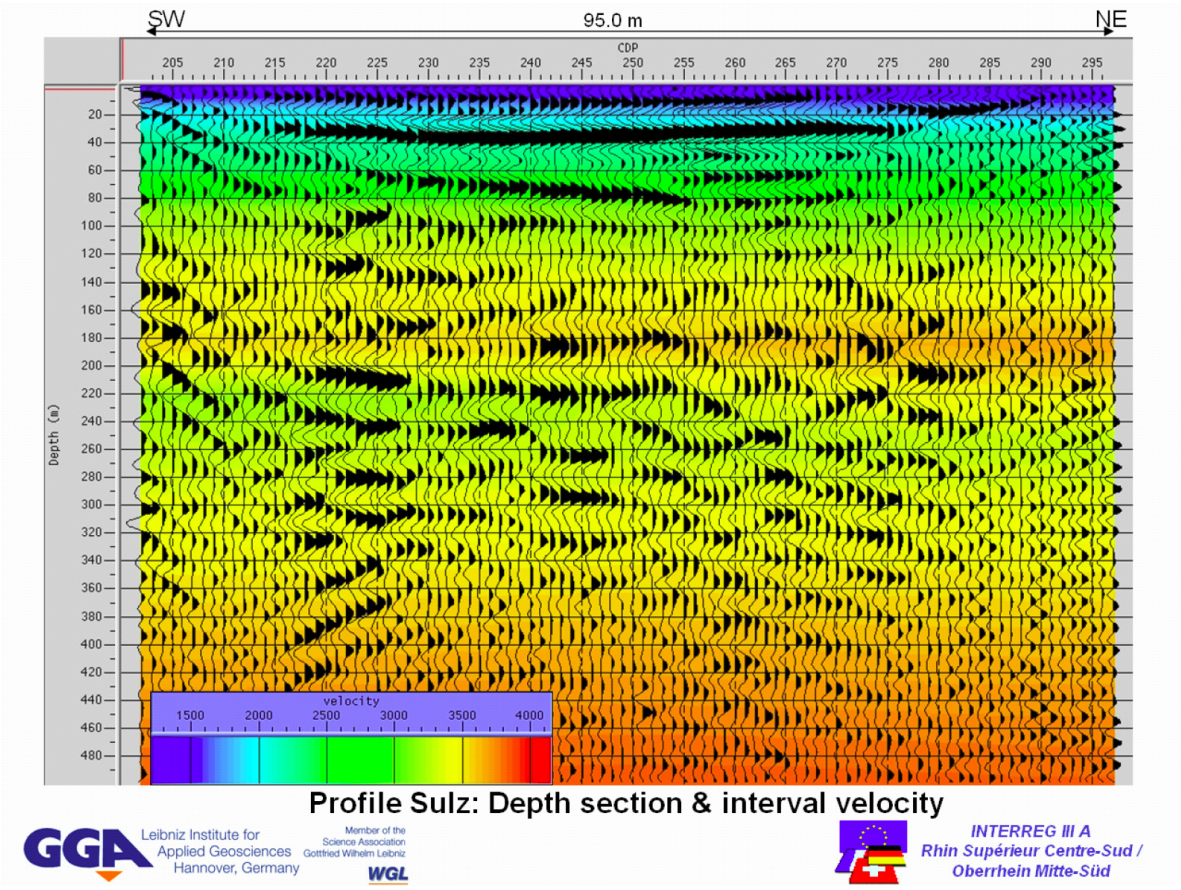

Figure 8: *S-wave velocity section obtained with S-wave reflection and refraction seismic measurement (Interreg III Project "Mikrozonierung am südlichen Oberrhein", U. Polom, unpublished results.*

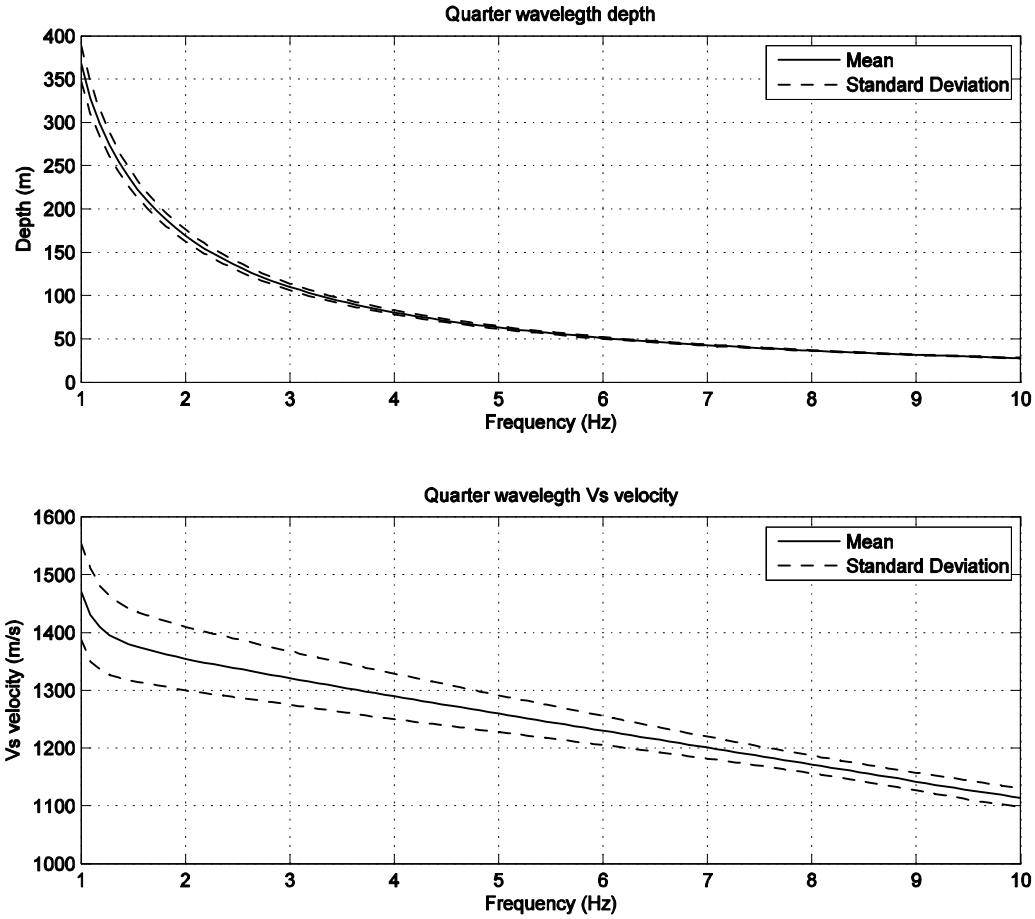

Figure 9: *Quarter wavelength and quarter-wavelength velocity as a function of frequency at the site of the arrays at Sulz.*

Finally Figure 9 provides the quarter-wavelength velocities and depth as function of frequency for the ambient vibration array measurements. The seismic station SULZ is located on rock. Table 2 summarizes the mean velocity for different thicknesses. The average velocity is computed in a way such that the travel-time in an average model corresponds to the sum of the travel times in the single layers:

$$\frac{1}{\bar{v}} = \frac{1}{H}\sum_{i=1}^{n}\frac{h_i}{v_i} \qquad \text{with} \qquad H = \sum_{i=1}^{n} h_i \,.$$

H [m]	Vs mean [m/s]	Vs stddev [m/s]
5	872	70
10	938	26
20	1040	22
30	1130	13
40	1188	15
50	1226	21
(100)	(1311)	(41)

Table 2: *Mean S-wave velocity at Sulz over the thickness H.*

6. Results obtained with SPAC

In case of SULZ, SPAC was applied to the vertical component of motion acquired at the larger subarray (334m aperture). The resulting dispersion density is depicted in Figure 10. The dashed line is the picked dispersion curve that is used for the inversion afterwards. The resolution limits were estimated from the scatter of the dispersion density plot and from the shape of the SPAC functions. Generally, SPAC curve should follow zero-order Bessel function. The scatter in the 1-3.5 Hz frequency band is relatively low. Two examples of SPAC curves are depicted in Figure 11. The contributions of SPAC functions to the dispersion density region specified by thin black lines (stable, well defined ridge in dispersion density plot, see Fig. 10) are denoted by black color. SPAC curves do not deviate from the shape of Bessel function in these intervals (especialy for ring 7). Several ring layouts were also tested with very similar results. Large scatter of dispersion density and SPAC functions which do not fit Bessel's function preclude an estimation of dispersion curve at frequencies higher than 3.5Hz.
To conclude: Using SPAC, it was possible to identify a relatively strong dispersive signal on the vertical component in the frequency band 1-3.5Hz.

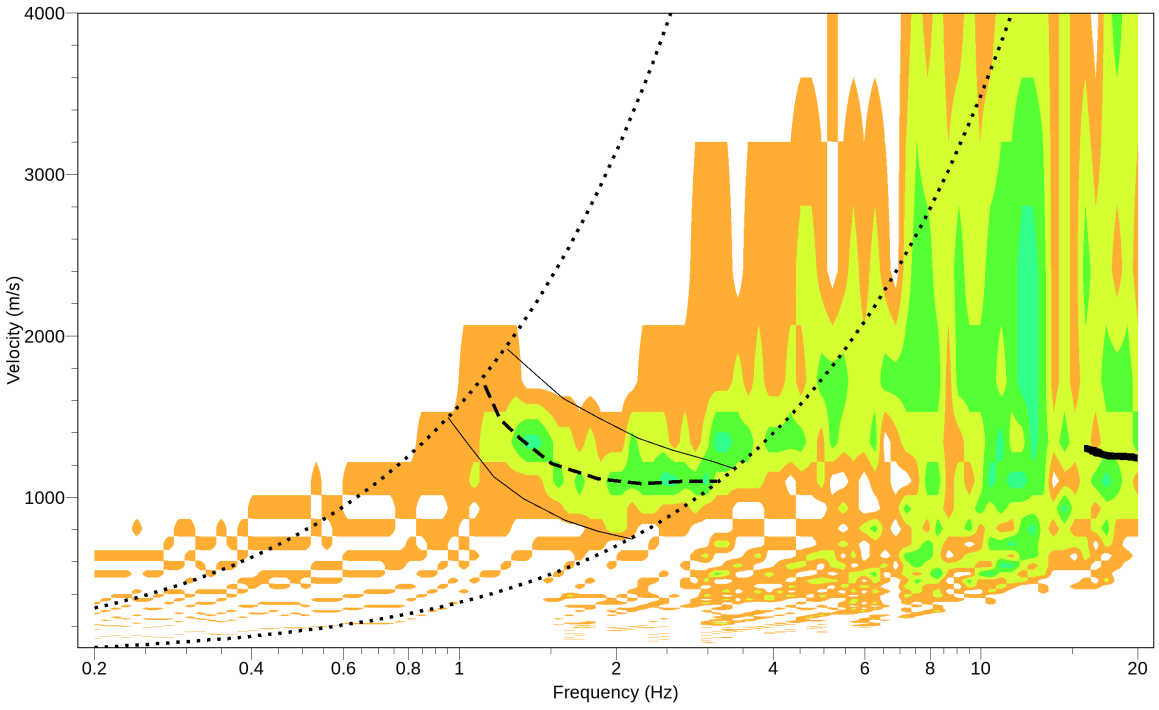

Figure 10: *Dispersion density grid (stack of dispersion solutions obtained from different rings) with picked dispersion curve (dashed line), and a chunk of the dispersion curve obtained from HRBF (thick solid line). A stable zone of higher dispersion density is delineated with thin black lines. The dotted lines represent the wave-number limits deduced from the observations.*

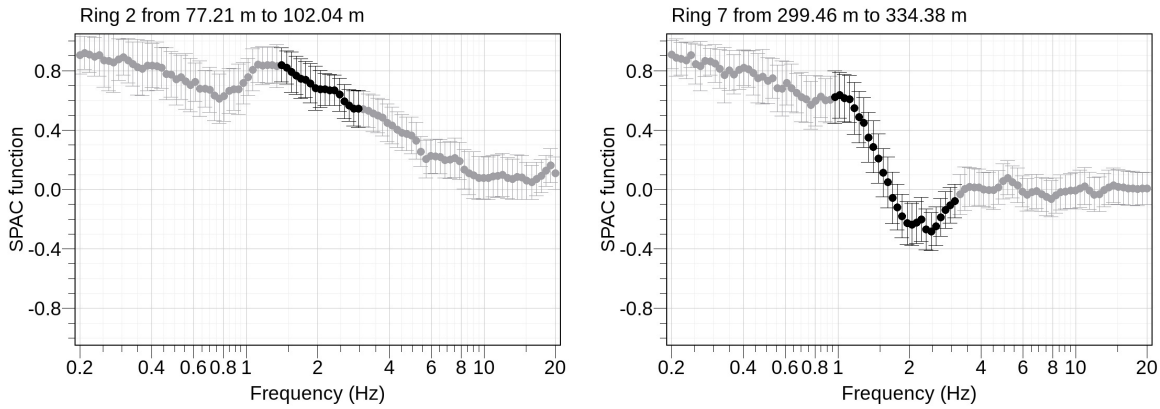

Figure 11: *An example of SPAC curves for two rings (small ring on the left, large ring on the right).*

If we assume that the results from SPAC are reliable, then we see a segment of the Rayleigh fundamental mode. In this case it is suggested that HRBF analysis provides parts of the dispersion curves of higher modes (see the results for Love waves in Figure 12 and compare to Figure 7), and almost no information for the fundamental mode. Assigning mode numbers to the different segments is difficult. However we have repeated the inversion using the results from SPAC, the H/V curve and assuming that one of the segments seen for Love waves belong to the third or fourth higher mode. We also defined a range of possible velocity for the upper layer. The new inverted profiles are shown in Figure 13 (blue, cyan and red).

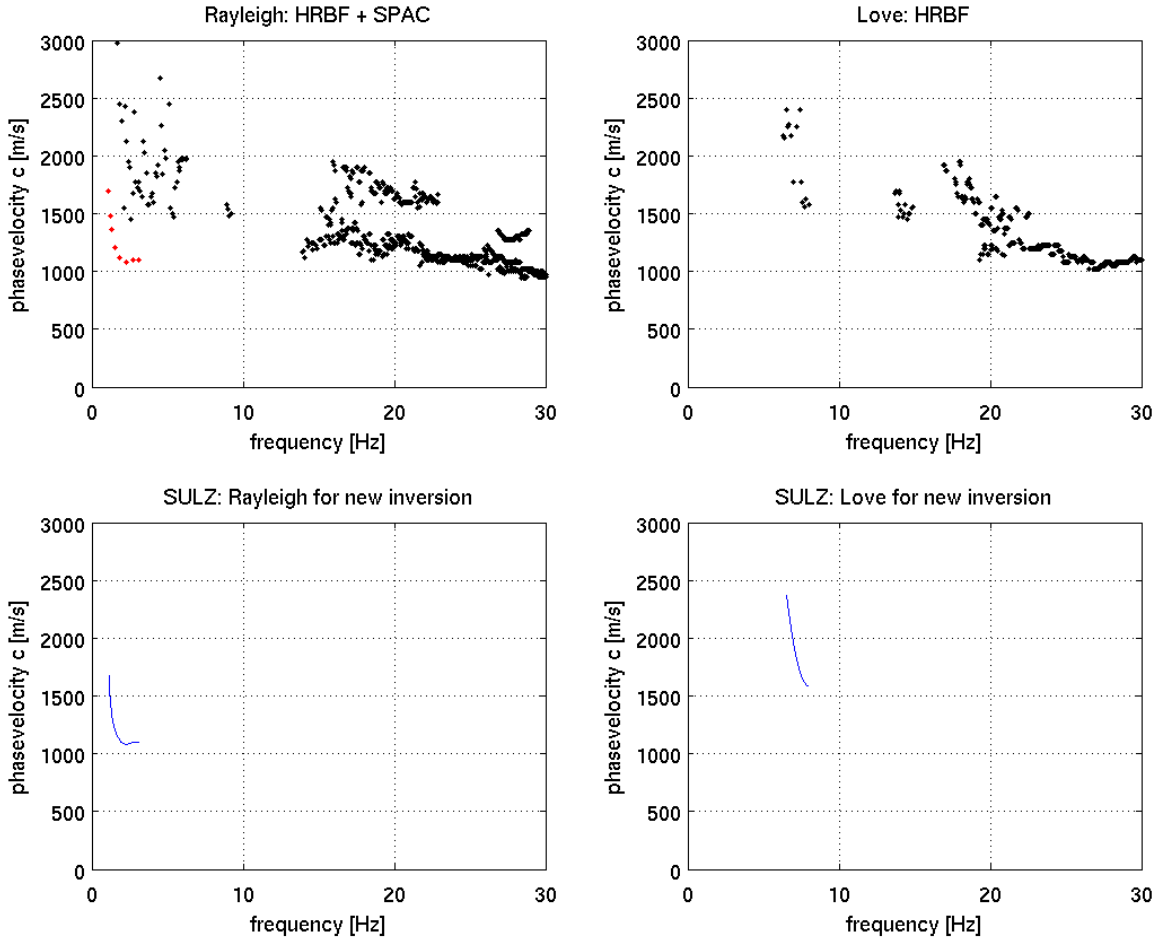

Figure 12: *The upper two pictures show the dispersion-curves obtained with HRBF (black) and SPAC (red). Below, the segments used for the new inversions are plotted in blue.*

In Figure 13, the inverted profiles using only the HRBF-results are shown in green. The new profiles using also the SPAC-results for the inversion are shown in blue (Love-segment was assigned to the fourth higher mode), cyan (Love-segment was also assigned to the fourth higher mode, very good fit of the Rayleigh fundamental mode segment) and red (Love-segment was assigned to the third higher mode).

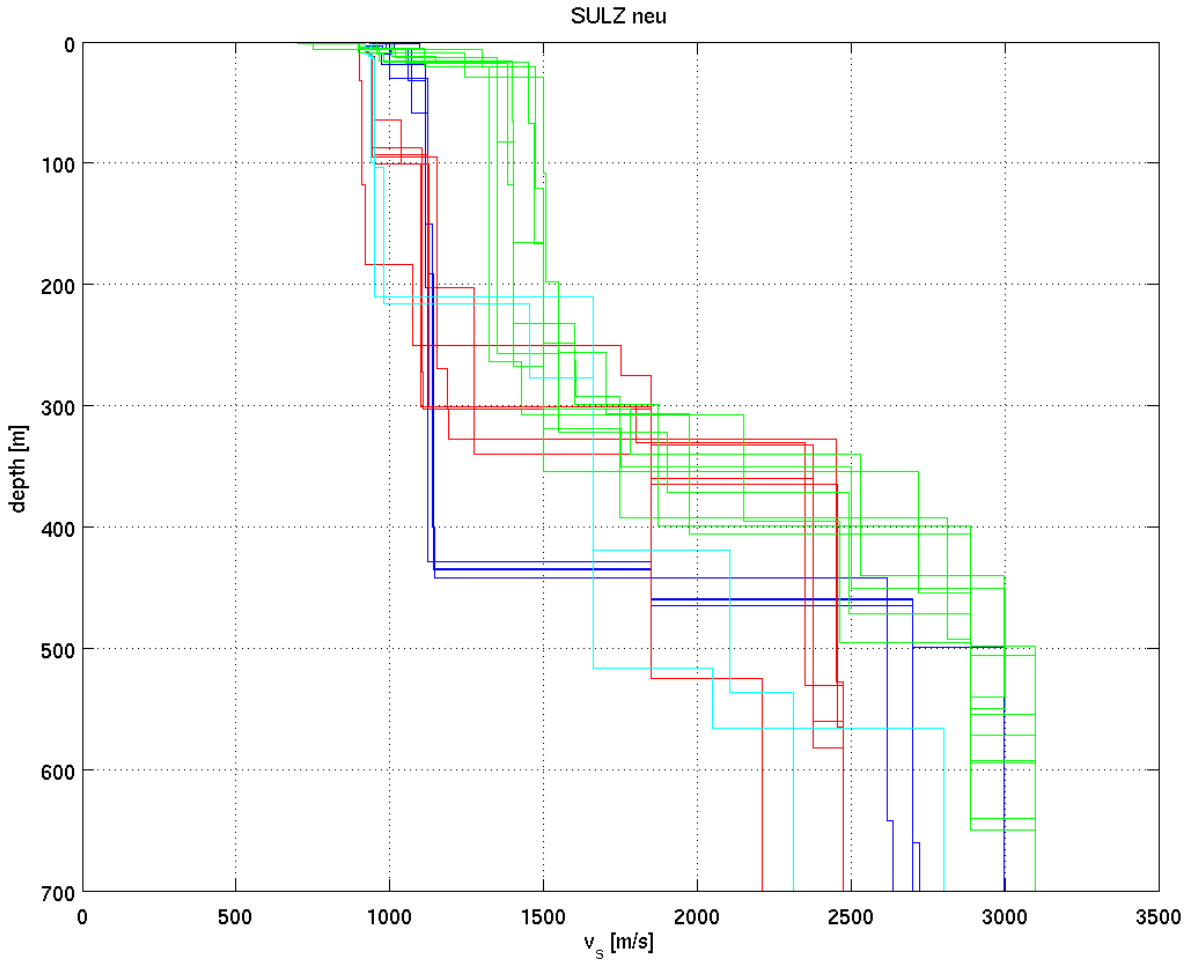

Figure 13: *This picture shows the inverted profiles using only the HRBF-results (green) as well as the new ones (blue, cyan and red). For all new models we assumed that the Rayleigh-segment obtained from SPAC is part of the fundamental mode. The Love-segment was once assigned to the third higher mode (red) and once to the fourth higher mode (blue and cyan). The cyan models show a very well fit of the Rayleigh fundamental mode segment.*

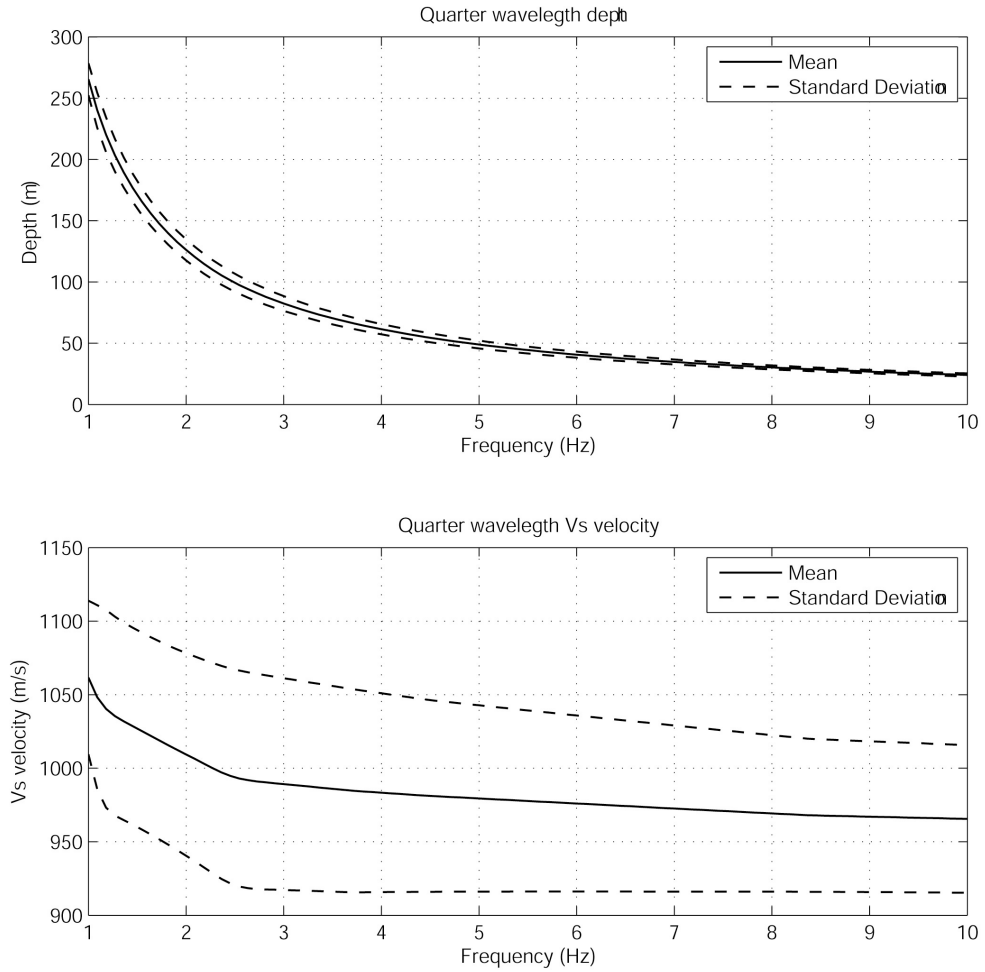

Figure 14: *Quarter wavelength and quarter wavelength velocity as a function of frequency at the site of the arrays at Sulz, using only the new inverted profiles obtained with the SPAC-results (blue, cyan and red in fig. 13).*

H [m]	Vs mean [m/s]	Vs stddev [m/s]
5	951	46
10	956	48
20	962	49
30	968	52
40	975	58
50	979	62
100	995	71
150	1020	66
200	1035	65
400	(1170)	(39)

Table 3: *Mean S-wave velocity at Sulz over the thickness H, when using only profiles obtained with the SPAC-results (blue, cyan and red in fig. 13).*

7. References

Aki K. (1957). Space and time spectra of stationary stochastic waves, with special reference to microtremors. Bull. Earthq. Res. Inst. 35, 415–456.

Asten, M.W. (2006). On bias and noise in passive seismic data from finite circular array data processed using SPAC methods, Geophysics, 71, 153-162.

Bettig, B., Bard, P. Y., Scherbaum, F., Riepl, J., Cotton, F., Cornou, C., and Hatzfeld, D., 2001, Analysis of dense array noise measurements using the modified spatial auto-correlation method (SPAC) Application to the Grenoble area: Bollettino di GeofisicaTeorica dApplicata, 42, 281–304.

Capon, J., (1969). High-resolution frequency-wave number spectrum analysis, Proc. IEEE, 57(8), 1408-1418.

Fäh, D., Kind, F. and Giardini, D. (2001). A theoretical investigation of average H/V ratios. Geophys. J. Int., 145, 535-549.

Fäh, D., Kind, F. and Giardini, D., (2003). Inversion of local A-wave velocity structures from average H/V ratios, and their use for the estimation of site-effects, J. Seismol., 7, 449-467.

Fäh, D., Stamm, G. and Havenith, H.-B., (2008). Analysis of three-component ambient vibration array measurements, Geophys. J. Int., 172, 199-213.

Kind, F., Fäh, D. and Giardini, D., (2005). Array measurements of S-wave velocities from ambient vibrations, Geophys. J. Int., 160, 114-126.

Wathelet M., Jongmans D., Ohrnberger M. (2005). Direct inversion of spatial auto correlation curves with the neighborhood algorithm. Bull. Seismol. Soc. Am. 95,1787–1800.

Yamanaka, H., Takemura, M., Ishida, H. and Niea, M. (1994). Characteristics of long-period micro-tremors and their applicability in exploration of deep layers. Bull. Seism. Soc. Am., 84, 1831-1841